

Article

Not peer-reviewed version

Radiative Corrections to the Nucleon Isovector g_V and g_A

[Oleksandr Tomalak](#)* and Yi-Bo Yang

Posted Date: 12 March 2026

doi: 10.20944/preprints202603.0931.v1

Keywords: nucleon structure; axial-vector coupling constant; neutron decay; QED; QCD; lattice QCD; electroweak radiative corrections



Preprints.org is a free multidisciplinary platform providing preprint service that is dedicated to making early versions of research outputs permanently available and citable. Preprints posted at Preprints.org appear in Web of Science, Crossref, Google Scholar, Scilit, Europe PMC.

Copyright: This open access article is published under a [Creative Commons CC BY 4.0 license](#), which permit the free download, distribution, and reuse, provided that the author and preprint are cited in any reuse.

Disclaimer/Publisher's Note: The statements, opinions, and data contained in all publications are solely those of the individual author(s) and contributor(s) and not of MDPI and/or the editor(s). MDPI and/or the editor(s) disclaim responsibility for any injury to people or property resulting from any ideas, methods, instructions, or products referred to in the content.

Article

Radiative Corrections to the Nucleon Isovector g_V and g_A

Oleksandr Tomalak ^{1,*}  and Yi-Bo Yang ^{1,2,3,4} 

¹ Institute of Theoretical Physics, Chinese Academy of Sciences, Beijing 100190, China

² University of Chinese Academy of Sciences, School of Physical Sciences, Beijing 100049, China

³ School of Fundamental Physics and Mathematical Sciences, Hangzhou Institute for Advanced Study, UCAS, Hangzhou 310024, China

⁴ International Centre for Theoretical Physics Asia-Pacific, Beijing/Hangzhou, China

* Correspondence: tomalak@itp.ac.cn

Abstract

Electroweak, QCD, and QED radiative corrections to the nucleon low-energy coupling constants g_V and g_A are enhanced by large perturbative logarithms between the electroweak and hadronic scale, as well as between the hadronic scale and the low-energy MeV scale. Additionally, higher-order pion-mass splitting corrections to the nucleon axial-vector charge might be large. By consistently incorporating these effects, we provide an updated relation between the lattice-QCD and physical g_A , finding a total radiative correction of 3.5(2.1)% (5.6(7)%). This leads to an expected lattice-QCD result of $g_A^{\text{QCD}} = 1.265(26)$ ($g_A^{\text{QCD}} = 1.240(9)$) when based on a combination of lattice-QCD and data-driven (or only data-driven) inputs, respectively. Future phenomenological, chiral perturbation theory, and lattice-QCD studies can improve both the central value and the uncertainty of this estimate.

Keywords: nucleon structure; axial-vector coupling constant; neutron decay; QED; QCD; lattice QCD; electroweak radiative corrections

1. Introduction

Low-energy charged-current electroweak processes involving nucleons, such as neutron beta decay and inverse beta decay (antineutrino-proton scattering), are characterized by the Fermi coupling constant, the Cabibbo-Kobayashi-Maskawa matrix element V_{ud} , and the nucleon isovector vector g_V and axial-vector g_A coupling constants. These processes are now measured with extraordinary precision, with state-of-the-art results provided by the UCN τ [1], PERKEO-III [2,3], and JUNO [4–7] collaborations. For example, the neutron lifetime is known at the 2×10^{-4} level [1], and reactor antineutrino experiments such as JUNO are providing increasingly precise data [4,7].

At this level of experimental accuracy, electroweak, quantum chromodynamics (QCD), and quantum electrodynamics (QED) radiative corrections become essential for extracting fundamental parameters from data [8–11]. The dominant theoretical uncertainty in these corrections originates from hadronic contributions, whose precise determination remains a central challenge in modern electroweak and hadronic physics [8,12–22]. Remarkably, first-principles lattice-QCD simulations are being used now to compute these hadronic effects [18,19], enabling, for instance, a determination of g_V using only Standard Model inputs [8].

The next major milestone is the first-principles determination of g_A within the Standard Model. Achieving this goal requires precise relations that connect lattice-QCD quantities to their experimentally measured counterparts, a topic of active research [8,9,23,24]. A proposed relation based on the heavy-baryon chiral perturbation theory (HBChPT) [23] suggested that radiative corrections are dominated by leading order (LO) and next-to-leading order (NLO) HBChPT contributions. Subsequent analysis [9] expressed all LO and NLO HBChPT contributions in terms of matrix elements of quark

currents, presented contributions from scales above the energy of hadronic physics, and discussed renormalization group evolution between the scale of hadronic physics and MeV energy.

In this short note, we numerically analyze large logarithms and hadronic contributions in radiative corrections to g_A . We show that the dominant electroweak, QCD, and QED corrections to both g_V and g_A are governed by large perturbative logarithms as well as leading and next-to-leading-order HBChPT contributions from Ref. [23]. To guide future Standard Model determinations of g_A , we present an updated numerical evaluation of radiative corrections.

2. Materials and Methods

We begin our analysis of radiative corrections to g_V and g_A by identifying the leading contributions enhanced by large logarithms. The dominant part of these corrections arises from universal logarithms between the electroweak scale and hadronic scale, as well as between the hadronic scale and the characteristic MeV scale of experiment. In the leading-logarithm (LL) approximation, the corrections at the electron mass scale $\mu_\chi = m_e$ are [8,9,12]

$$\delta g_V^{\text{LL}}(\mu_\chi = m_e) = \frac{\delta g_A^{\text{LL}}(\mu_\chi = m_e)}{g_A^{(0)}} = \frac{\alpha}{\pi} \left(\ln \frac{M_Z}{\mu_0} - \frac{\alpha_S}{4\pi} \ln \frac{M_W}{\mu_0} + \frac{3}{4} \ln \frac{\mu_0}{m_e} \right) \approx 2.36(2)\%, \quad (1)$$

with the electromagnetic coupling constant α and the strong coupling constant α_S . M_W and M_Z denote the electroweak-scale masses of the W and Z bosons, respectively, the hadronic scale is taken as $\mu_0 \approx m_N$, with the nucleon mass m_N , and $g_A^{(0)} \approx 1.27$ [23] denotes the axial-vector charge in the chiral limit without radiative corrections. To estimate the associated uncertainty, we vary μ_0 within the range $\left[\frac{m_N}{\sqrt{2}}, \sqrt{2}m_N \right]$ and show the dependence of these LL results on the hadronic scale μ_0 in Figure 1.

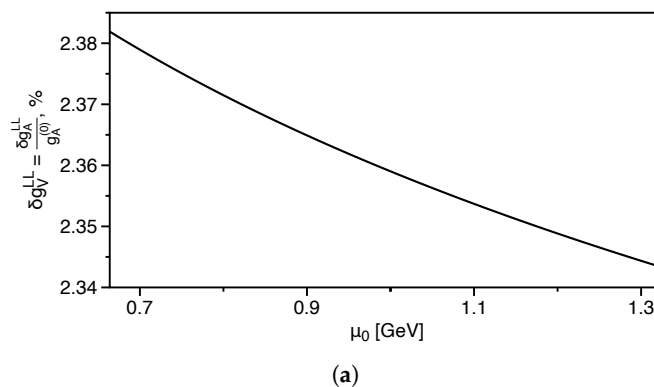


Figure 1. Perturbatively improved relative radiative correction to the nucleon low-energy coupling constants $\delta g_V^{\text{LL}}(\mu_\chi = m_e)$ and $\frac{\delta g_A^{\text{LL}}(\mu_\chi = m_e)}{g_A^{(0)}}$ is shown as a function of the hadronic scale μ_0 .

The full one-loop result for the radiative correction becomes independent of the scale μ_0 once the relevant hadronic contributions are taken into account. In the following, we illustrate this explicitly for the vector coupling constant. The one-loop result including the leading QCD logarithm $\delta g_V^{1\text{-loop+LL}}$ is obtained by accounting for the constant term and hadronic corrections in Eq. (1) as

$$\delta g_V^{1\text{-loop+LL}}(\mu_\chi = m_e) = \frac{\alpha}{\pi} \left(\ln \frac{M_Z}{\mu_0} - \frac{\alpha_S}{4\pi} \ln \frac{M_W}{\mu_0} + \frac{3}{4} \ln \frac{\mu_0}{m_e} \right) - \frac{5\alpha}{16\pi} - e^2 \int \frac{id^4q}{(2\pi)^4} \frac{v^2 + Q^2}{Q^4} \frac{\bar{T}_3(v, Q^2)}{2m_N v}, \quad (2)$$

where we take the strong coupling constant α_S at the electroweak matching scale. Here, $Q^2 = -q^2$ denotes the virtuality, and $v = v \cdot q = q^0$ is the energy transfer in the nucleon rest frame, with $v = (1, 0, 0, 0)$. The nucleon spin-independent forward Compton scattering invariant amplitude in the

isoscalar channel \bar{T}_3 is subtracted at large Q^2 using a μ_0 -dependent operator product expansion (OPE) term [8]:

$$\bar{T}_3(v, Q^2) = T_3(v, Q^2) - \frac{4}{3} \frac{m_{NV}}{Q^2 + \mu_0^2} \left(1 - \frac{\alpha_S}{\pi}\right). \quad (3)$$

The constant term $-\frac{5\alpha}{16\pi}$ yields -0.073% , while the hadronic contribution for $\mu_0 = m_N$ is evaluated as $0.156(12)\%$ [8,12–17,20]. The resulting correction to the vector coupling constant is

$$\delta g_V^{1\text{-loop}+\text{LL}}(\mu_\chi = m_e) = 2.444(12)\%, \quad (4)$$

which is independent of the hadronic scale μ_0 . The resummation of leading logarithms and inclusion of next-to-leading logarithmic corrections increases the radiative correction to the vector coupling constant by 0.055% . Adding also the uncertainty estimate by varying the matching scales and the hadronic scale μ_0 , we obtain

$$\delta g_V(\mu_\chi = m_e) = 2.499(13)\%. \quad (5)$$

In complete analogy with Eq. (2), the one-loop radiative correction to the axial-vector coupling constant, including the leading QCD logarithm, $\delta g_A^{1\text{-loop}+\text{LL}}$ can be written as [9]

$$\frac{\delta g_A^{1\text{-loop}+\text{LL}}(\mu_\chi = m_e)}{g_A^{(0)}} = \frac{\alpha}{\pi} \left(\ln \frac{M_Z}{\mu_0} - \frac{\alpha_S}{4\pi} \ln \frac{M_W}{\mu_0} + \frac{3}{4} \ln \frac{\mu_0}{m_e} \right) - \frac{5\alpha}{16\pi} + \frac{\delta g_A^{\text{extra}}}{g_A^{(0)}} + \frac{2e^2}{g_A^{(0)}} \int \frac{id^4q}{(2\pi)^4} \left(\frac{v^2 - 2Q^2}{3Q^2} \frac{\bar{S}_1(v, Q^2)}{Q^2} - \frac{v^2}{Q^2} \frac{S_2(v, Q^2)}{m_{NV}} \right), \quad (6)$$

$$\frac{\delta g_A^{\text{extra}}}{g_A^{(0)}} = \frac{\Delta \bar{g}_A^{\text{QCD}+\text{QED}}(\lambda_\gamma, \mu_0)}{g_A^{(0)}} + e^2 \int \frac{id^4q}{(2\pi)^4} \frac{2\bar{m}t_{VP}(q, v) - \bar{t}_{VA}(q, v)}{q^2 - \lambda_\gamma^2}. \quad (7)$$

The OPE-subtracted nucleon spin-dependent forward Compton scattering invariant amplitudes in the isovector channel \bar{S}_1 and S_2 yield a correction of $0.169(6)\%$ [25] for $\mu_0 = m_N$. The term $\delta g_A^{\text{extra}}$, often omitted in precise evaluations [25], must be included for a complete result. Here, $\Delta \bar{g}_A^{\text{QCD}+\text{QED}}(\lambda_\gamma, \mu_0)$ is the OPE-subtracted QED radiative correction to the nucleon matrix element of the axial-vector quark current, evaluated in the Feynman gauge, $\xi = 1$,¹ with infrared regularization by the photon mass λ_γ . The integral of the second term in $\delta g_A^{\text{extra}}$ involves OPE-subtracted two-current correlation functions: vector-pseudoscalar t_{VP} , with the isospin-averaged quark mass \bar{m} , and vector-axial-vector \bar{t}_{VA} , that cancel both the infrared divergence and residual μ_0 dependence from $\Delta \bar{g}_A^{\text{QCD}+\text{QED}}(\lambda_\gamma, \mu_0)$. The explicit definitions for hadronic objects t_{VP} and \bar{t}_{VA} are presented in Ref. [9].

The term $\delta g_A^{\text{extra}}$ can be evaluated solely in lattice QCD. However, it is instructive to discuss dominant contributions to this object. First, the leading contributions in $\delta g_A^{\text{extra}}$ from one-pion intermediate states together with a corresponding dependence on the nucleon isovector magnetic moment, cancel exactly between two terms in $\delta g_A^{\text{extra}}$ [9]. Two-pion intermediate states generate a large logarithm as

¹ An extra term has to be added to relate $\Delta \bar{g}_A^{\text{QCD}+\text{QED}}(\lambda_\gamma, \mu_0)$ to the OPE-subtracted QED radiative correction in an arbitrary R_ξ gauge $\Delta \bar{g}_A^{\text{QCD}+\text{QED}}(\xi, \lambda_\gamma, \mu_0)$,

$$\frac{\Delta \bar{g}_A^{\text{QCD}+\text{QED}}(\lambda_\gamma, \mu_0)}{g_A^{(0)}} = \frac{\Delta \bar{g}_A^{\text{QCD}+\text{QED}}(\xi, \lambda_\gamma, \mu_0)}{g_A^{(0)}} + \frac{1 - \xi}{2} \frac{\alpha}{\pi} \left[\ln \frac{\lambda_\gamma^2}{\mu_0^2} + \frac{a\xi \ln(a\xi)}{1 - a\xi} \right], \quad (8)$$

with the arbitrary parameter a that enters the gauge-dependent piece of the photon propagator as $1/(q^2 - a\xi\lambda_\gamma^2)$.

well as the next-to-leading order contribution, expressed in terms of the NLO HBChPT low-energy coupling constants (LECs) c_3 and c_4 , as

$$\begin{aligned} \frac{\delta g_A^{\text{extra}}}{g_A^{(0)}} &\approx \frac{Z_\pi \left[1 + 3(g_A^{(0)})^2\right]}{2} \frac{\alpha}{\pi} \ln \frac{m_N}{m_\pi} + 2\alpha Z_\pi m_\pi \left[c_4 - c_3 + \frac{3}{8m_N} + \frac{9}{16} \frac{(g_A^{(0)})^2}{m_N} \right] \\ &+ \frac{\delta g_A^{\text{extra,N}}}{g_A^{(0)}} + \dots \approx \begin{cases} 2.9(3)\%, & c_4^{\text{N}^3\text{LO}} - c_3^{\text{N}^3\text{LO}} \\ 2.2(2)\%, & c_4^{\text{NLO}} - c_3^{\text{NLO}} \\ 1.6(1)\%, & c_4^{\text{Born}} - c_3^{\text{Born}} \\ 0.7(2.1)\%, & (2c_4 - c_3)^{\text{LQCD}} - c_4^{\text{N}^3\text{LO}} \end{cases} + \frac{\delta g_A^{\text{extra,N}}}{g_A^{(0)}} + \dots, \end{aligned} \quad (9)$$

where we have chosen the nucleon mass as the ultraviolet cutoff in the logarithmic term, and m_π denotes the pion mass. The uncertainty is estimated by adding, in quadrature, the power-counting uncertainty of the NLO contribution to the uncertainty on the coupling constant $c_4 - c_3$. The parameter $Z_\pi \approx 0.81$ is the QED isospin-breaking LEC responsible for the electromagnetic pion-mass splitting.

The NLO HBChPT LECs c_3 and c_4 enter the second term. Phenomenological determinations from πN scattering data [26,27] provide the following values (errors added in quadrature):

$$c_3^{\text{NLO}} = -3.61(5) \text{ GeV}^{-1}, \quad c_4^{\text{NLO}} = 2.17(3) \text{ GeV}^{-1}, \quad c_4^{\text{NLO}} - c_3^{\text{NLO}} = 5.78(6) \text{ GeV}^{-1}, \quad (10)$$

$$c_3^{\text{N}^3\text{LO}} = -5.61(6) \text{ GeV}^{-1}, \quad c_4^{\text{N}^3\text{LO}} = 4.26(4) \text{ GeV}^{-1}, \quad c_4^{\text{N}^3\text{LO}} - c_3^{\text{N}^3\text{LO}} = 9.87(7) \text{ GeV}^{-1}. \quad (11)$$

The fit results change significantly going from NLO to N²LO but stabilize at N³LO [26,27]. Since our calculation is performed at NLO in HBChPT, we estimate the systematic uncertainty from the difference between the NLO and the more complete N³LO values (rather than using N²LO). The combination $2c_4^{\text{NLO}} - c_3^{\text{NLO}} = 7.95(8) \text{ GeV}^{-1}$ ($2c_4^{\text{N}^3\text{LO}} - c_3^{\text{N}^3\text{LO}} = 14.13(10) \text{ GeV}^{-1}$) can also be extracted from the m_π^3 dependence of the nucleon axial-vector charge g_A . However, a recent lattice-QCD calculation [28] gives a value an order of magnitude smaller $(2c_4 - c_3)^{\text{LQCD}} = 0.85(25) \text{ GeV}^{-1}$. Using this lattice-QCD result together with the phenomenological extraction of c_3 or c_4 as an input, we obtain the relevant combination of LECs $c_4 - c_3 = (2c_4 - c_3)^{\text{LQCD}} - c_4^{\text{NLO}} = -1.32(25) \text{ GeV}^{-1}$ and $c_4 - c_3 = (2c_4 - c_3)^{\text{LQCD}} - c_4^{\text{N}^3\text{LO}} = -3.41(25) \text{ GeV}^{-1}$. For the central value of the QED correction with lattice-QCD input $(2c_4 - c_3)^{\text{LQCD}}$, we adopt the LEC $c_4^{\text{N}^3\text{LO}}$: $c_4 - c_3 = (2c_4 - c_3)^{\text{LQCD}} - c_4^{\text{N}^3\text{LO}} = -3.4(13.3) \text{ GeV}^{-1}$, and assign a systematic uncertainty by taking the difference with the value obtained from the largest alternative combination. Within the Born approximation of the nucleon intermediate state only for expressions in Appendix D of Ref. [9], we evaluate the LECs of interest as²

$$c_3^{\text{Born}} = \frac{(g_A^{(0)})^2}{4m_N} - \left[\frac{3}{2} + (g_A^{(0)})^2 \right] (g_A^{(0)})^2 \frac{\pi m_\pi}{(4\pi F_\pi)^2} = -1.2(4) \text{ GeV}^{-1}, \quad (12)$$

$$c_4^{\text{Born}} = -\frac{(g_A^{(0)})^2}{4m_N} + \left[1 + (g_A^{(0)})^2 \right] (g_A^{(0)})^2 \frac{\pi m_\pi}{(4\pi F_\pi)^2} = 0.9(2) \text{ GeV}^{-1}, \quad (13)$$

with the pion decay constant $F_\pi \approx 92.4 \text{ MeV}$, and estimate the error as the nucleon state contribution to these LECs. The Born result for $2c_4^{\text{Born}} - c_3^{\text{Born}} = 3.0(8) \text{ GeV}^{-1}$ is also in tension both with lattice QCD [28] and fits to the experimental data [26,27]. Thus, it is worthwhile to explore whether additional combinations of c_3 and c_4 can be constrained using the light-quark mass dependence of isoscalar nucleon charges, such as isoscalar scalar charge, as well as to determine c_3 and c_4 directly from nucleon matrix elements as described in Appendix D of Ref. [9]. Isovector charges have been precisely

² The other NLO HBChPT LECs are $c_2^{\text{Born}} = -\frac{3}{8} \frac{(g_A^{(0)})^2}{m_N} + \frac{\pi m_\pi}{(4\pi F_\pi)^2} = -0.3(1)$ and $\kappa_1^{\text{Born}} = \frac{m_\pi}{4\pi F_\pi} \frac{m_N}{F_\pi} = 1.9(3)$.

determined from lattice QCD in Ref. [29]. Moreover, a lattice-QCD determination of $\delta g_A^{\text{extra}}$ would directly constrain the low-energy coupling constant $c_4 - c_3$ and clarify the HBChPT convergence pattern.

For estimating the size of hadronic corrections, we separate the Born contribution from nucleon states, $\delta g_A^{\text{extra,N}}$, in Eq. (9), and indicate inelastic contributions as According to evaluations of typical hadronic objects in Refs. [8,30–33], the nucleon intermediate state contribution is either dominant or has a comparable size to inelastic excitations. We get $-0.0127(2)\%$ and $0.222(3)\%$ for the nucleon-state contribution to two terms in $\delta g_A^{\text{extra}}$ of Eq. (7), respectively. We describe the details of this calculation in Appendix A and investigate Ward identities for the nucleon state by evaluating hadronic objects from an alternative decomposition of radiative corrections in Appendix B.

Accounting for the constant term and the hadronic contribution from the second line of Eq. (6), we obtain the one-loop radiative correction, including the leading QCD logarithm, to the axial-vector coupling constant $\delta g_A^{1\text{-loop+LL}}$,

$$\frac{\delta g_A^{1\text{-loop+LL}}(\mu_\chi = m_e)}{g_A^{(0)}} = 2.457(6)\% + \frac{\delta g_A^{\text{extra}}}{g_A^{(0)}} = \begin{cases} 5.5(7)\%, & c_4^{\text{N}^3\text{LO}} - c_3^{\text{N}^3\text{LO}} \\ 4.9(7)\%, & c_4^{\text{NLO}} - c_3^{\text{NLO}} \\ 4.3(4)\%, & c_4^{\text{Born}} - c_3^{\text{Born}} \\ 3.4(2.1)\%, & (2c_4 - c_3)^{\text{LQCD}} - c_4^{\text{N}^3\text{LO}} \end{cases}. \quad (14)$$

For the uncertainty estimate in the first two lines (the third line), we add 0.2% uncertainty from the variation of the hadronic scale under the logarithm in Eq. (9) to 0.7% difference between the results with NLO and N³LO couplings (0.1% from the nucleon state contribution in $c_4^{\text{Born}} - c_3^{\text{Born}}$) and to 0.3% difference in the evaluation of the nucleon intermediate state contribution between Appendix A and Appendix B in quadrature, respectively. Compared to previous estimates [25], this analysis consistently incorporates the large logarithmic enhancements at the one-loop level, explicitly accounts for contributions from all two- and three-current correlation functions, and includes the associated uncertainty.

As in the case of the vector coupling constant, we further include the next-to-leading logarithmic corrections and resummation, and obtain³

$$\frac{\delta g_A(\mu_\chi = m_e)}{g_A^{(0)}} = 2.513(8)\% + \frac{\delta g_A^{\text{extra}}}{g_A^{(0)}} = \begin{cases} 5.6(7)\%, & c_4^{\text{N}^3\text{LO}} - c_3^{\text{N}^3\text{LO}} \\ 5.0(7)\%, & c_4^{\text{NLO}} - c_3^{\text{NLO}} \\ 4.4(4)\%, & c_4^{\text{Born}} - c_3^{\text{Born}} \\ 3.5(2.1)\%, & (2c_4 - c_3)^{\text{LQCD}} - c_4^{\text{N}^3\text{LO}} \end{cases}. \quad (16)$$

3. Results and Discussion

It is instructive to separate the contributions from the uncertain $c_4 - c_3$, the remaining uncertain hadronic corrections, and the precisely calculable perturbative contribution. The resulting radiative correction can be decomposed into three terms:

$$\frac{g_A}{g_A^{\text{QCD}} g_V} - 1 = -0.033(15)\% + 2\alpha Z_\pi m_\pi (c_4 - c_3) + \frac{\delta g_A^{\text{had}}}{g_A^{\text{QCD}} g_V}, \quad (17)$$

³ For reference, we also present the correction δg_A at the chiral scale of the nucleon mass

$$\frac{\delta g_A(\mu_\chi = m_N)}{g_A^{(0)}} = \begin{cases} 4.2(7)\%, & c_4^{\text{N}^3\text{LO}} - c_3^{\text{N}^3\text{LO}} \\ 3.6(7)\%, & c_4^{\text{NLO}} - c_3^{\text{NLO}} \\ 3.0(4)\%, & c_4^{\text{Born}} - c_3^{\text{Born}} \\ 2.1(2.1)\%, & (2c_4 - c_3)^{\text{LQCD}} - c_4^{\text{N}^3\text{LO}} \end{cases}. \quad (15)$$

where g_A^{QCD} denotes the axial-vector charge in the isospin limit. The first term contains the difference of γW box contributions to g_A and g_V , as well as higher-order remnants.⁴ The second term depends on the combination $c_4 - c_3$ of the NLO HBChPT LECs c_3 and c_4 . This term has a sizable uncertainty as discussed in the previous section, with the coefficient $2\alpha Z_\pi m_\pi = 0.16(2)$ GeV and an uncertainty estimate from the HBChPT power counting. The third term represents the hadronic contributions $\delta g_A^{\text{extra}}$ but explicitly removes the dependence on $c_4 - c_3$,

$$\frac{\delta g_A^{\text{had}}}{g_A^{\text{QCD}} g_V} = \frac{\delta g_A^{\text{extra}}}{g_A^{\text{QCD}} g_V} - 2\alpha Z_\pi m_\pi (c_4 - c_3) \approx 1.5(4)\%. \quad (18)$$

The corresponding uncertainty is given by 0.3% difference in the evaluation of the nucleon intermediate state contribution between Appendix A and Appendix B and 0.2% uncertainty from the variation of the hadronic scale under the logarithm in Eq. (9) added in quadrature. The correction in Eq. (17) does not depend on the scale and is free from large logarithms of Eq. (1).

For various $c_4 - c_3$ inputs considered above, we obtain

$$\frac{g_A}{g_A^{\text{QCD}} g_V} - 1 = \begin{cases} 3.0(7)\%, & c_4^{\text{N}^3\text{LO}} - c_3^{\text{N}^3\text{LO}} \\ 2.3(7)\%, & c_4^{\text{NLO}} - c_3^{\text{NLO}} \\ 1.8(4)\%, & c_4^{\text{Born}} - c_3^{\text{Born}} \\ 0.8(2.1)\%, & (2c_4 - c_3)^{\text{LQCD}} - c_4^{\text{N}^3\text{LO}} \end{cases}. \quad (19)$$

As our final result for relating lattice-QCD determinations to experimental measurements, we quote Eq. (19). Based on the current experimental value of the axial-vector to vector coupling constant ratio $\frac{g_A}{g_V} = 1.2753(13)$ [36] and N³LO LECs [26,27], we expect the lattice-QCD result for the axial-vector charge $g_A^{\text{QCD}} = 1.240(9)$. Exploiting the strong lattice-QCD constraint on NLO HBChPT LECs and estimating the systematic uncertainty by taking the largest difference between alternative inputs, we get $g_A^{\text{QCD}} = 1.265(26)$.

We present our results for the nucleon axial-vector charge in Figure 2 and compare them to the Flavour Lattice Averaging Group (FLAG) average of lattice-QCD calculations [37–51], which itself comprises data from both 2+1+1 and 2+1 flavour simulations distinguishing between calculations with and without a dynamical charm quark in the sea. We find a tension between our result based on N³LO fits for the coupling constants c_3 and c_4 and modern lattice-QCD determinations. Including the lattice-QCD constraint on $2c_4 - c_3$ [28] and inflating the error bars or estimating the LECs c_3 and c_4 within the Born approximation removes the tension. This situation underscores the need for a direct lattice-QCD determination of the hadronic QED corrections to g_A and/or for improved lattice-QCD constraints on the next-to-leading-order HBChPT low-energy coupling constants c_3 and c_4 , as well as for improvements in phenomenological and ChPT analyses.

⁴ Explicitly, these remnants are $\frac{\delta g_A - \delta g_A^{\text{extra}}}{g_A^{(0)} g_V} \left(\frac{g_A^{(0)}}{g_A^{\text{QCD}}} - 1 \right) = -0.110\%$, where we take the HBChPT input from Refs. [34,35], $\left| \frac{\delta g_A - \delta g_A^{\text{extra}} - (g_V - 1)}{g_A^{(0)} g_V} \left(\frac{1}{g_V} - 1 \right) \right| < 0.0004\%$, and $-\frac{C_\beta^r - 1}{g_V} \left(\frac{C_\beta^r - 1 - \delta g_A}{g_A^{\text{QCD}}} - 1 \right) = (0.058 - 0.075)\%$ for a range of values $\delta g_A^{\text{extra}}$ in this work. $C_\beta^r = 1 + \mathcal{O}(\alpha)$ is the semileptonic Wilson coefficient in the low-energy effective field theory of quarks and leptons, evaluated at the GeV renormalization scale.

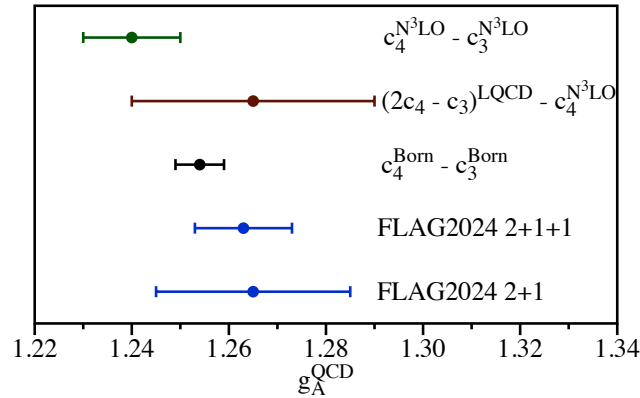


Figure 2. The expected lattice-QCD result for the nucleon axial-vector charge, based on the experimental measurements of g_A [36] and up-to-date radiative corrections evaluated in this work, is compared to the Flavour Lattice Averaging Group (FLAG) average of lattice-QCD calculations [37–51]. The results of this work are presented for three cases: using NLO HBChPT coupling constants in radiative corrections from $N^3\text{LO}$ fits to πN scattering data; incorporating the available lattice-QCD constraint from Ref. [28]; and using estimates from the Born approximation.

Author Contributions: All authors have read and agreed to the published version of the manuscript.

Funding: This research was funded by the National Science Foundation of China under Grants No. 12347105, 12525504, 12293060, 12293062, and 12447101.

Data Availability Statement: No new data were created.

Acknowledgments: Wolfram Mathematica [54] and DataGraph [55] were extremely useful in this work.

Conflicts of Interest: The authors declare no conflicts of interest.

Abbreviations

The following abbreviations are used in this manuscript:

FLAG	Flavour Lattice Averaging Group
HBChPT	Heavy Baryon Chiral Perturbation Theory
LEC	Low-Energy Coupling constant
LL	Leading Logarithm
LO	Leading Order
LQCD	Lattice Quantum ChromoDynamics
NLO	Next-to-Leading Order
MeV	MegaelectronVolt
OPE	Operator Product Expansion
QCD	Quantum ChromoDynamics
QED	Quantum ElectroDynamics

Appendix A. Nucleon-State Contribution to $\delta g_A^{\text{extra}}$

In this Appendix, we present the evaluation of the nucleon-state contribution $\delta g_A^{\text{extra,N}}$ to $\delta g_A^{\text{extra}}$ in Eq. (7):

$$\begin{aligned} \frac{\delta g_A^{\text{extra}}}{g_A^{(0)}} = & \left[\frac{e^2 \bar{m} b_\rho b_\lambda}{g_A^{(0)}} \int \frac{id^4 q}{(2\pi)^4} \frac{g_{\mu\nu} \left(\bar{F}_{AVV}^{\mu\nu\lambda\rho}(q, v) + \bar{F}_{AVV,0}^{\mu\nu\lambda\rho}(q, v) \right)}{q^2 - \lambda_\gamma^2} + 2i\pi\delta(v \cdot r) \Delta_{\text{em}} m_N \right] \Big|_{r_\lambda=0} \\ & + e^2 \int \frac{id^4 q}{(2\pi)^4} \frac{2\bar{m} t_{VP}(q, v) - \bar{t}_{VA}(q, v)}{q^2 - \lambda_\gamma^2}, \end{aligned} \quad (\text{A1})$$

with the momentum insertion in the axial-vector current r_λ , an arbitrary vector $b: b^2 = -1, b \cdot v = 0$, and the nucleon electromagnetic correction to the isospin-averaged nucleon mass,

$$\Delta_{\text{em}} m_N = -\frac{e^2}{2} \int \frac{d^4 q}{(2\pi)^4} \frac{g_{\mu\nu} \left(\tau_{VV}^{\mu\nu}(q, v) + \tau_{VV,0}^{\mu\nu}(q, v) \right)}{q^2}. \quad (\text{A2})$$

The pure imaginary term $2i\pi\delta(v \cdot r)\Delta_{\text{em}} m_N$ cancels the nucleon pole singularity from t_{AVV} . The hadronic objects t_{AVV} (τ_{VV}) are defined in terms of the axial-vector quark bilinear and two vector currents (two vector currents) in Ref. [9].

We describe the evaluation of $\Delta_{\bar{g}_A^{\text{QCD+QED}}}$ in Appendix A.1, while the contribution from the nucleon two-current correlation function $2\bar{m}t_{VP} - \bar{t}_{VA}$ is presented in Appendix A.2.

Appendix A.1. Contribution from Three-Current Correlation Functions

The nucleon-state contribution from three-current correlation functions in Eq. (A1) can be expressed as

$$\begin{aligned} & \frac{\alpha}{8\pi} \int \frac{dQ^2}{\beta m_N^2} \left[\frac{1 - 2\beta^3 + \beta^4}{1 + \beta} F_1^p F_1^n + \frac{1 - \beta}{1 + \beta} \left(1 + \frac{\beta}{2} \right) \left[F_1^p F_2^n + F_1^n F_2^p \right] + \frac{1 + \beta + \beta^3}{(1 + \beta)^2} F_2^p F_2^n \right] \\ & = -0.0127(2)\%, \end{aligned} \quad (\text{A3})$$

with the dimensionless parameter $\beta = \sqrt{1 + \frac{4m_N^2}{Q^2}}$, exploiting the standard notations for nucleon form factors and fits to the experimental data from Ref. [52].

Appendix A.2. Contribution from Two-Current Correlation Functions

We express the contribution from \bar{t}_{VA} in terms of the nucleon form factors as

$$-e^2 \int \frac{id^4 q}{(2\pi)^4} \frac{\bar{t}_{VA}(q, v)}{q^2} \rightarrow -\frac{\alpha}{12\pi} \int \frac{dQ^2}{m_N^2} \frac{1 - \beta}{1 + \beta} \left(\beta + \frac{1}{2} \right) \frac{G_M^V F_A}{g_A^{(0)}} = 0.144(3)\%, \quad (\text{A4})$$

exploiting the nucleon axial-vector form factor from Ref. [53].

Corrections from the integral of t_{VP} beyond the leading pion-pole contribution $t_{VP}^{1\pi}$ are chirally suppressed [9], i.e.,

$$e^2 \int \frac{id^4 q}{(2\pi)^4} \frac{2\bar{m}(t_{VP}(q, v) - t_{VP}^{1\pi}(q, v))}{q^2 - \lambda_\gamma^2} = \frac{\alpha}{\pi} \mathcal{O} \left(\frac{m_\pi^2}{m_N^2}, \frac{m_\pi^2}{(4\pi F_\pi)^2} \right) \lesssim 0.006\%. \quad (\text{A5})$$

It is instructive to analyze also the expression in terms of the nucleon form factors for the nucleon-state contribution from t_{VP} ,

$$e^2 \int \frac{id^4 q}{(2\pi)^4} \frac{2\bar{m}t_{VP}(q, v)}{q^2 - \lambda_\gamma^2} \rightarrow \frac{\alpha}{4\pi} \int \frac{dQ^2}{Q^2} \left(\frac{1 - \beta}{1 + \beta} F_1^V + \frac{5 + 4\beta}{3(1 + \beta)^2} F_2^V \right) \frac{F_A - \frac{Q^2}{2m_N^2} F_P}{g_A^{(0)}}. \quad (\text{A6})$$

The F_2^V term yields 0.046%. The leading pion-pole contribution $t_{VP}^{1\pi}$ is included as a part of the nucleon form factors. Subtracting it from Eq. (A6), we obtain the finite nucleon-state contribution from t_{VP} : 0.078%.

Appendix B. Alternative Decomposition and Ward Identities

In this Appendix, we present the evaluation of the nucleon-state contribution $\delta g_A^{\text{extra,N}}$ to $\delta g_A^{\text{extra}}$ expressed in terms of alternative hadronic objects as

$$\frac{\delta g_A^{\text{extra}}}{g_A^{(0)}} = e^2 \int \frac{id^4q}{(2\pi)^4} \frac{2\bar{m}t_{VP}(q, v)}{q^2 - \lambda_\gamma^2} + \frac{\Delta_{\text{em}}m_N}{m_N} - \frac{\alpha}{8\pi} + \left[\frac{e^2\bar{m}b_\rho b_\lambda}{g_A^{(0)}} \frac{\partial}{\partial r_\lambda} \left(\int \frac{id^4q}{(2\pi)^4} \frac{g_{\mu\nu} \left(t_{PVV}^{\mu\nu\rho}(r, q, v) + t_{PVV,0}^{\mu\nu\rho}(r, q, v) \right)}{q^2 - \lambda_\gamma^2} \right) + 2i\pi\delta(v \cdot r)\Delta_{\text{em}}m_N \right] \Big|_{r_\lambda=0}, \quad (\text{A7})$$

with the momentum insertion in the pseudoscalar density r_λ . The hadronic objects t_{PVV} are defined in terms of the pseudoscalar quark bilinear and two vector currents in Ref. [9].

We describe the evaluation of the integral from the nucleon three-current correlation functions in Appendix B.1, while the contribution from the nucleon two-current correlation functions is presented in Appendix B.2. In Appendix B.3, we compare the results from Appendix A and Appendix B.

Appendix B.1. Contribution from Three-Current Correlation Functions

The nucleon-state contribution from three-current correlation functions in Eq. (A7) can be expressed as

$$\frac{\alpha}{8\pi} \int \frac{dQ^2}{\beta m_N^2} \frac{1-\beta}{1+\beta} \left[(1-\beta)(1+\beta)^2 F_1^p F_1^n + \left(1-\beta - \frac{3}{2}\beta^2 \right) [F_1^p F_2^n + F_1^n F_2^p] - (1+2\beta) F_2^p F_2^n \right] = -0.1558(5)\%. \quad (\text{A8})$$

Appendix B.2. Contribution from Two-Current Correlation Functions

Corrections from t_{VP} are described in Appendix A.2, while additional two-current corrections correspond to the relative Born contribution to the isospin-averaged nucleon mass. We update the value according to Ref. [33] 0.017(1)% with a new result 0.0166(2)%.

Appendix B.3. Discussion of Ward Identities

After adding the nucleon-state contribution of Eq. (A8) and the constant term in Eq. (A7) to the nucleon-state terms in the isospin-averaged nucleon mass shift, the difference to Eq. (A1) is 0.30% that is an expected order of magnitude for inelastic contributions. We exploit this number for uncertainty estimates.

References

1. Gonzalez, F. M.; et al. (UCN τ Collaboration). Improved neutron lifetime measurement with UCN τ . *Phys. Rev. Lett.* **2021**, *127*, 162501.
2. Märkisch, B.; et al. Measurement of the weak axial-vector coupling constant in the decay of free neutrons using a pulsed cold neutron beam. *Phys. Rev. Lett.* **2019**, *122*, 242501.
3. Dubbers, D.; Saul, H.; Märkisch, B.; Soldner, T.; Abele, H. Exotic decay channels are not the cause of the neutron lifetime anomaly. *Phys. Lett. B* **2019**, *791*, 6–10.
4. An, F.; et al. (JUNO Collaboration). Neutrino physics with JUNO. *J. Phys. G* **2016**, *43*, 030401.
5. Abusleme, A.; et al. (JUNO Collaboration). JUNO physics and detector. *Prog. Part. Nucl. Phys.* **2022**, *123*, 103927.
6. Abusleme, A.; et al. (JUNO Collaboration). Sub-percent precision measurement of neutrino oscillation parameters with JUNO. *Chin. Phys. C* **2022**, *46*, 123001.
7. Abusleme, A.; et al. (JUNO Collaboration). First measurement of reactor neutrino oscillations at JUNO. *arXiv:2511.14593*.
8. Cirigliano, V.; Dekens, W.; Mereghetti, E.; Tomalak, O. Effective field theory for radiative corrections to charged-current processes: vector coupling. *Phys. Rev. D* **2023**, *108*, 053003.

9. Cirigliano, V.; Dekens, W.; Mereghetti, E.; Tomalak, O. Effective field theory for radiative corrections to charged-current processes. II. Axial-vector coupling. *Phys. Rev. D* **2025**, *111*, 053005.
10. Tomalak, O. Theory of inverse beta decay for reactor antineutrinos. *arXiv:2512.07956*.
11. Tomalak, O. On radiative corrections to inverse beta decay at low energies. *arXiv:2512.07957*.
12. Marciano, W. J.; Sirlin, A. Improved calculation of electroweak radiative corrections and the value of V_{ud} . *Phys. Rev. Lett.* **2006**, *96*, 032002.
13. Seng, C.-Y.; Gorchtein, M.; Ramsey-Musolf, M. J. Dispersive evaluation of the inner radiative correction in neutron and nuclear β decay. *Phys. Rev. D* **2019**, *100*, 013001.
14. Seng, C.-Y.; Gorchtein, M.; Patel, H. H.; Ramsey-Musolf, M. J. Reduced hadronic uncertainty in the determination of V_{ud} . *Phys. Rev. Lett.* **2018**, *121*, 241804.
15. Czarnecki, A.; Marciano, W. J.; Sirlin, A. Radiative corrections to neutron and nuclear beta decays revisited. *Phys. Rev. D* **2019**, *100*, 073008.
16. Hayen, L. Standard model $\mathcal{O}(\alpha)$ renormalization of g_A and its impact on new physics searches. *Phys. Rev. D* **2021**, *103*, 113001.
17. Shiells, K.; Blunden, P. G.; Melnitchouk, W. Electroweak axial structure functions and improved extraction of the V_{ud} CKM matrix element. *Phys. Rev. D* **2021**, *104*, 033003.
18. Feng, X.; Gorchtein, M.; Jin, L.-C.; Ma, P.-X.; Seng, C.-Y. First-principles calculation of electroweak box diagrams from lattice QCD. *Phys. Rev. Lett.* **2020**, *124*, 192002.
19. Ma, P.-X.; et al. Lattice QCD calculation of electroweak box contributions to superallowed nuclear and neutron beta decays. *Phys. Rev. Lett.* **2024**, *132*, 191901.
20. Gorbahn, M.; Moretti, F.; Jäger, S. Beyond leading logarithms in g_V : the semileptonic weak Hamiltonian at $\mathcal{O}(\alpha\alpha_s^2)$. *arXiv:2510.27648*.
21. Crosas, Ó. L.; Mereghetti, E. Radiative corrections to superallowed beta decays at $\mathcal{O}(\alpha^2 Z)$. *JHEP* **2026**, *02*, 114.
22. Cao, Z.; Hill, R. J.; Plestid, R.; Vander Griend, P. The $Z\alpha^2$ correction to superallowed beta decays in effective field theory and implications for $|V_{ud}|$. *arXiv:2511.05446*.
23. Cirigliano, V.; de Vries, J.; Hayen, L.; Mereghetti, E.; Walker-Loud, A. Pion-induced radiative corrections to neutron β decay. *Phys. Rev. Lett.* **2022**, *129*, 121801.
24. Seng, C.-Y. Hybrid analysis of radiative corrections to neutron decay with current algebra and effective field theory. *JHEP* **2024**, *07*, 175.
25. Gorchtein, M.; Seng, C.-Y. Dispersion relation analysis of the radiative corrections to g_A in neutron β decay. *JHEP* **2021**, *10*, 053.
26. Hoferichter, M.; Ruiz de Elvira, J.; Kubis, B.; Meissner, U. Matching pion-nucleon Roy-Steiner equations to chiral perturbation theory. *Phys. Rev. Lett.* **2015**, *115*, 192301.
27. Hoferichter, M.; Ruiz de Elvira, J.; Kubis, B.; Meissner, U. Roy-Steiner-equation analysis of pion-nucleon scattering. *Phys.Rept.* **2016**, *625*, 1-88.
28. Hall, Zack B.; et al. Signs of Non-Monotonic Finite-Volume Corrections to g_A . *arXiv:2503.09891*.
29. Wang, J.; Hu, Zh.; Ji, X.; Jiang, X.; Su, Y.; Sun, P.; Yang, Y. Precision determination of nucleon iso-vector scalar and tensor charges at the physical point. *arXiv:2511.02326*.
30. Tomalak, O.; Pasquini, B.; Vanderhaeghen, M. Two-photon exchange contribution to elastic e^- -proton scattering: Full dispersive treatment of πN states and comparison with data. *Phys. Rev. D* **2017**, *96*, 096001.
31. Tomalak, O.; Vanderhaeghen, M. Dispersion relation formalism for the two-photon exchange correction to elastic muon-proton scattering: elastic intermediate state. *Eur. Phys. J. C* **2018**, *78*, 514.
32. Tomalak, O. Two-Photon Exchange Correction to the Lamb Shift and Hyperfine Splitting of S Levels. *Eur. Phys. J. A* **2019**, *55*, 64.
33. Tomalak, O. Electromagnetic proton-neutron mass difference. *Eur. Phys. J. Plus* **2020**, *135*, 411.
34. Kambor, J.; Mojzis, M. Field redefinitions and wave function renormalization to $\mathcal{O}(p^{**4})$ in heavy baryon chiral perturbation theory. *JHEP* **1999**, *04*, 031.
35. Bernard, V.; Meissner, U. The Nucleon axial-vector coupling beyond one loop. *Phys. Lett. B* **2006**, *639*, 278-282.
36. Navas, S. Review of particle physics. *Phys. Rev. D* **2024**, *110*, 030001.
37. Aoki, Y.; et al. FLAG review 2024. *Phys. Rev. D* **2026**, *113*, 014508.
38. Chang, C. C. et al. A per-cent-level determination of the nucleon axial coupling from quantum chromodynamics. *Nature* **2018**, *558*, 91-94.
39. Walker-Loud, A. et al. Lattice QCD Determination of g_A . *PoS* **2020**, *CD2018*, 020.

40. Jang, Y.-C.; Gupta, R.; Bhattacharya, T.; Yoon, B.; Lin, H.-W. [Precision Neutron Decay Matrix Elements (PNDME)]d Nucleon isovector axial form factors. *Phys. Rev. D* **2024**, *109*, 014503.
41. Alexandrou, C.; Bacchio, S.; Constantinou, M.; Finkenrath, J.; Frezzotti, R.; Kostrzewa, B.; Koutsou, G.; Spanouides, G.; Urbach, C. [Extended Twisted Mass] Nucleon axial and pseudoscalar form factors using twisted-mass fermion ensembles at the physical point. *Phys. Rev. D* **2024**, *109*, 034503.
42. Liang, J.; Yang, Y.-B.; Draper, T.; Gong, M.; Liu, K.-F. Quark spins and Anomalous Ward Identity. *Phys. Rev. D* **2018**, *98*, 074505.
43. Park, S.; Gupta, R.; Yoon, B.; Mondal, S.; Bhattacharya, T.; Jang, Y.-C.; Joo, B.; Winter, F. [Nucleon Matrix Elements (NME)] Precision nucleon charges and form factors using (2+1)-flavor lattice QCD. *Phys. Rev. D* **2022**, *105*, 054505.
44. Smail, R. E. et al. [QCDSF/UKQCD/CSSM] Constraining beyond the standard model nucleon isovector charges. *Phys. Rev. D* **2023**, *108*, 094511.
45. Bali, G. S.; Collins, S.; Heybrock, S.; Löffler, M.; Rödl, R.; Söldner, W.; Weishäupl, S. [RQCD] Octet baryon isovector charges from $N_f=2+1$ lattice QCD. *Phys. Rev. D* **2023**, *108*, 034512.
46. Djukanovic, D.; von Hippel, G.; Meyer, H. B.; Ottnad, K.; Wittig, H. Improved analysis of isovector nucleon matrix elements with $N_f=2+1$ flavors of $O(a)$ improved Wilson fermions. *Phys. Rev. D* **2024**, *109*, 074507.
47. Harris, T.; von Hippel, G.; Junnarkar, P.; Meyer, H. B.; Ottnad, K.; Wilhelm, J.; Wittig, H.; Wrang, L. Nucleon isovector charges and twist-2 matrix elements with $N_f = 2 + 1$ dynamical Wilson quarks. *Phys. Rev. D* **2019**, *100*, 034513.
48. Bali, G. S.; Barca, L.; Collins, S.; Gruber, M.; Löffler, M.; Schäfer, A.; Söldner, W.; Wein, P.; Weishäupl, S.; Wurm, T. [RQCD] Nucleon axial structure from lattice QCD. *JHEP* **2020**, *05*, 126.
49. Djukanovic, D.; von Hippel, G.; Koponen, J.; Meyer, H. B.; Ottnad, K.; Schulz, T.; Wittig, H. Isovector axial form factor of the nucleon from lattice QCD. *Phys. Rev. D* **2022**, *106*, 074503.
50. Gupta, R.; Jang, Y.-C.; Yoon, B.; Lin, H.-W.; Cirigliano, V.; Bhattacharya, T. Isovector Charges of the Nucleon from $2+1+1$ -flavor Lattice QCD. *Phys. Rev. D* **2018**, *98*, 034503.
51. Bhattacharya, T.; Cirigliano, V.; Cohen, S.; Gupta, R.; Joseph, A.; Lin, H.-W.; Yoon, B. [PNDME] Iso-vector and Iso-scalar Tensor Charges of the Nucleon from Lattice QCD. *Phys. Rev. D* **2015**, *92*, 094511.
52. Borah, K.; Hill, R. J.; Lee G.; Tomalak, O. Parametrization and applications of the low- Q^2 nucleon vector form factors. *Phys. Rev. D* **2020**, *102*, 074012.
53. Cai, T.; et al. Measurement of the axial vector form factor from antineutrino–proton scattering. *Nature* **2023**, *614*, 7946, 48–53.
54. Wolfram Research, Inc. *Mathematica*, Version 12.2.0.0; Wolfram Research, Inc.: Champaign, IL, USA, 2022.
55. MacAskill, M.R. DataGraph. *J. Stat. Softw.* **2012**, *47*, 1–9.

Disclaimer/Publisher’s Note: The statements, opinions and data contained in all publications are solely those of the individual author(s) and contributor(s) and not of MDPI and/or the editor(s). MDPI and/or the editor(s) disclaim responsibility for any injury to people or property resulting from any ideas, methods, instructions or products referred to in the content.